Self-organization in active fluids: A new class of turbulence

V. Bratanov[1], F. Jenko[2] and E. Frey[3]

[1]Max Planck Institute for Plasma Physics, Boltzmannstr. 2, 85748 Garching, Germany
[2]Department of Physics and Astronomy, University of California, Los Angeles, California 90095, USA
[3]Arnold Sommerfeld Center for Theoretical Physics and Center for NanoScience, Department of Physics, Ludwig-Maximilians-Universität München, Theresienstr. 37, 80333 München, Germany

Significance statement

It is widely appreciated that turbulence is one of the main challenges of modern theoretical physics. While up to now, most work in this area has been dedicated to the study of Navier-Stokes flows, there exist numerous examples of systems which exhibit similar types of spatio-temporal chaos but are described by more complex nonlinear equations. One such problem of quickly growing scientific interest is turbulence in active fluids. We find that such systems can exhibit power law energy spectra with non-universal exponents as a result of nonlinear self-organization, defining a new class of turbulent flows.

Abstract

Turbulence is a fundamental and ubiquitous phenomenon in nature, occurring from astrophysical to biophysical scales. At the same time, it is widely recognized as one of the key unsolved problems in modern physics, representing a paradigmatic example of nonlinear dynamics far from thermodynamic equilibrium. While in the past, most theoretical work in this area has been devoted to Navier-Stokes flows, there is now a growing awareness of the need to extend the research focus to systems with more general patterns of energy injection and dissipation. This includes various types of complex fluids, plasmas, as well as active systems consisting of self-propelled particles, like dense bacterial suspensions. Recently, a continuum model has been proposed for such "living fluids" which is based on the Navier-Stokes equations, but extends them to include some of the most general terms admitted by the symmetry of the problem (see [Wensink *et al.*, PNAS 109:14308 (2012)]). This introduces a new cubic nonlinearity, related to the Toner-Tu theory of flocking, which can interact with the quadratic Navier-Stokes nonlinearity. We show that as a result of the subtle interaction between these two terms, the energy spectra at large spatial scales exhibit power laws which are not universal, but depend on both finite-size effects and physical parameters. Our combined numerical and analytical analysis reveals the origin of this effect and even provides a way to understand it quantitatively. Turbulence in active fluids, characterized by this kind of nonlinear self-organization, defines a new class of turbulent flows.

1 Introduction

Despite several decades of intensive research, turbulence – the irregular motion of a fluid, gas, or plasma – still defies a thorough understanding. It is a paradigmatic example of nonlinear dynamics and self-organization far from thermodynamic equilibrium, also closely linked to fundamental questions about irreversibility [1] and mixing.[2] The classical example of a turbulent system is a Navier-Stokes flow, with a single quadratic nonlinearity, well-separated drive and dissipation ranges, and an extended intermediate range of purely conservative scale-to-scale energy transfer.[3] However, many turbulent systems of scientific interest involve more general patterns of energy injection, transfer, and dissipation, and their systematic investigation has only just begun. A fascinating example of this kind of generalized turbulent dynamics can be observed in dense bacterial suspensions.[4] Although the motion of the individual swimmers in the background fluid takes place at Reynolds numbers well below unity, the coarse-grained dynamics of these self-propelled particles displays spatio-temporal chaos, i.e., turbulence.[5, 6, 7] Here, the correlation functions of the velocity and vorticity fields display some essential differences compared to their counterparts in classical fluid turbulence.[8, 9] Moreover, the collective motion of bacteria in such suspensions exhibits long-range correlations [10], appears to be driven by internal instabilities [11] and depends strongly also on physical parameters like the large-scale friction.[12] Such results challenge the orthodox understanding of turbulent motion and call for a detailed theoretical investigation. This point is reinforced by the fact that there exist many other systems with similar characteristics, including flows generated by space-filling fractal square grids [13], turbulent astrophysical [14] and laboratory [15] plasmas, as well as chemical reaction-diffusion processes.[16]

In the present work, we study – numerically as well as analytically – the spectral properties of a continuum model which has recently been suggested as a minimal phenomenological model to describe the collective dynamics of dense bacterial suspensions [4, 17, 18]. A basic assumption of the model is that at high concentrations the dynamics of bacterial flow may be described as an incompressible fluid obeying the following equation of motion for the velocity field $\mathbf{v}(\mathbf{x}, t)$:

$$\frac{\partial \mathbf{v}}{\partial t} + \lambda_0(\mathbf{v}\cdot\nabla)\mathbf{v} + \nabla p = -\Gamma_0\Delta\mathbf{v} - \Gamma_2\Delta^2\mathbf{v} - \mu(v)\mathbf{v}\,, \tag{1}$$

where $\mu(v) = \alpha + \beta|\mathbf{v}|^2$. In addition to the advective nonlinearity, $(\mathbf{v}\cdot\nabla)\mathbf{v}$, and pressure term, ∇p, familiar from the Navier-Stokes model, the equation also accounts for internal drive and dissipation processes. Interestingly, apart from the last term on the right hand side and the pressure term, Eq. (1) amounts to a straightforward multi-dimensional generalization of the Kuramoto-Sivashinsky (KS) equation. The one-dimensional version of the latter was first put forward for studying turbulence in magnetized plasmas [19, 20] and subsequently proved useful for the description of chemical reaction-diffusion processes [21, 22] and flame front propagation.[23] It is widely regarded as a prototypical example of "phase turbulence."[24] As a hallmark, if both kinetic parameters are positive (Γ_0, $\Gamma_2 > 0$), the KS equation is linearly unstable for a band of wave vectors k, similar to other paradigmatic models of nonlinear dynamics like, e.g., the Swift-Hohenberg model.[25] For active systems this feature is supposed to emulate energy input into the bacterial system through stress-induced instabilities [11]. This represents a fundamentally different situation compared to Navier-Stokes turbulence with external forcing where the characteristics of the latter can be changed at will and have been shown to influence the statistics of the velocity field.[26, 27] In order for the system

to be stable there must be nonlinear and dissipative terms which limit the growth of these linearly unstable modes. While in the KS equation dissipation is only due to the fourth-order derivative of the velocity field, Eq. (1) contains an additional dissipation mechanism mediated through the cubic nonlinearity on the right hand side, $-\mu(v)\mathbf{v}$. The latter term was originally introduced by Toner and Tu to account for a propensity of self-propelled rod-like objects to exhibit local polar order ("flocking").[28, 29] Taken together, the hydrodynamic model comprises some of the key features common to systems exhibiting meso-scale turbulence: The dynamics of the system results from the interplay between energy input due to a band of linearly unstable modes with the advective Navier-Stokes nonlinearity as well as with terms modeling flocking behavior and dissipation. These generic features are shared with more elaborate hydrodynamic models of active matter recently reviewed in Ref. [30]. Therefore, Eq. (1) serves as a simple but generic test case to address some of the fundamental questions in the field of active turbulence. By choosing the parameters in the equation differently one can reproduce several distinctive physical systems as explained in more detail in the table in Section S.1 in the Supplementary Material. First and foremost, the similarities and differences between low and high Reynolds number turbulence remain to be elucidated. In particular, there is still a lack of understanding of the energy flow between different length scales.

Here, we address the above questions by a systematic analysis of the turbulent features of Eq. (1) combining numerical and analytical approaches. Based on a spectral representation adopted from the theory of classical turbulence [31] we give a comprehensive picture of the spectral energy balance and thereby facilitate the understanding of the interactions among different spatial scales. Furthermore, with the aid of extensive numerical simulations we confirm the existence of a spectral power law at the largest scales of the system. The steepness of this power law is not universal but depends on the parameters of the system (both of the linear and nonlinear terms in Eq. (1)). The form of the energy spectrum of a turbulent system represents one of its central features. Recent theoretical results [32] relate it to the frictional drag between the system and the surrounding walls. This relations have also been experimentally confirmed for two-dimensional turbulence.[33] In the present work, insight into the remarkable feature of a variable spectral exponent is gained by analyzing the role of the different terms in the equation for the spectral energy balance. As expected for a two-dimensional incompressible fluid, there exists an inverse flow of energy from intermediate to large scales.[34] Nevertheless, in contrast to the picture of classical, fully-developed two-dimensional Navier-Stokes turbulence, there is no inertial range characterized by a constant energy flux. Instead, we find that at large scales, the Navier-Stokes energy flux is proportional to the product of the corresponding wave number and energy, with the proportionality factor, having the units of frequency, being constant for the whole range characterized by spectral self-similarity. This differs fundamentally from the classical Navier-Stokes case, where the proportionality factor is the inverse of the nonlinear eddy turn-over time which is, in turn, a function of wave number and energy. In the model at hand, this energy flux is balanced by a linear dissipation/injection and a cubic dissipation term. For the latter, we derive an analytic approximation which compares very favorably with the numerical results and allows for an analytic closure predicting the type of dependence of the power law on the model parameters that is also confirmed numerically.

2 Results

We have studied the two-dimensional version of the continuum model defined by Eq. (1) both analytically and numerically. In our computational approach we have implemented a pseudo-spectral code which computes the linear terms in Fourier space and the nonlinearities in real space. The details of this procedure are described in Section S.1 of the Supplemental Material. All numerical results reported in this paper employ a resolution of 1024 effective Fourier modes in each direction, unless stated otherwise. For the following analysis it is convenient to make a choice for the typical velocity, length and time scales, denoted as v_0, ℓ and τ, respectively. Those are quantities necessary for normalizing Eq. (1). We define the typical velocity as $v_0 := \sqrt{\Gamma_0^3/\Gamma_2}$. From the spectral representation $\gamma(k) := -\alpha + \Gamma_0 k^2 - \Gamma_2 k^4$ of the linear part of Eq. (1) one reads off the wave number of the fastest growing mode, $k_{\max} = \sqrt{\Gamma_0/(2\Gamma_2)}$, which suggests to define the characteristic length and time scale as $\ell = 5\pi/k_{\max}$ and $\tau = \ell/v_0$, respectively. Accordingly, the normalized form of the parameters Γ_0 and Γ_2 reduce to fixed numbers, i.e., $\Gamma_0\tau/\ell^2 = 1/(5\sqrt{2}\pi)$ and $\Gamma_2/(\ell v_0^3) \approx 9 \cdot 10^{-5}$. The normalization of Eq. (1) is explained in greater detail in Section S.1 of the Supplemental Material. The parameters β and λ_0 can still be chosen freely. The numerical results reported here are obtained with $\beta\tau v_0 = 0.5$ and $\lambda_0 = 3.5$. The normalization units used here are the same as the ones in Ref. [4], meaning that our parameters (with $\alpha = -1$ and up to the different sign of Γ_0) correspond to the bacterial suspension described there.

A snapshot of the real-space vorticity field obtained from a numerical solution of Eq. (1) in the turbulent regime is shown in Fig. 1. It makes evident the random distribution of vortices across the simulation domain. Moreover, the time evolution of the vortex configuration turns out to be strongly incoherent. Due to this highly nonlinear behavior, associated with spatio-temporal chaos, exhibited by the system, we refer to its dynamics as turbulent.

2.1 Spectral analysis

A detailed analysis of the turbulent dynamics described by Eq. (1) is facilitated by a Fourier analysis of the velocity field (see Section S.1 in the Supplemental Material). Specifically, we are interested in the flow of energy between different spatial scales mediated by the various terms in Eq. (1). For brevity we shall refer to $E_{\mathbf{k}} := \langle |\mathbf{v}_{\mathbf{k}}(t)|^2 \rangle/2$ as the energy of Fourier mode $\mathbf{k}$, where the brackets $\langle\cdot\rangle$ denote an ensemble average, equivalent to a time average for a statistically stationary state as discussed in Section S.1 in the Supplemental Material. The ensuing spectral energy balance equation reads

$$\partial_t E_{\mathbf{k}} = 2\gamma(k) E_{\mathbf{k}} + T_{\mathbf{k}}^{\mathrm{adv}} + T_{\mathbf{k}}^{\mathrm{cub}}, \tag{2}$$

with the advective and cubic nonlinear terms given by

$$T_{\mathbf{k}}^{\mathrm{adv}} = +\lambda_0 \,\mathrm{Re}\left[\sum_{\mathbf{p}} M_{ijl}(\mathbf{k}) \langle v^i_{-\mathbf{k}} v^l_{\mathbf{k}-\mathbf{p}} v^j_{\mathbf{p}} \rangle\right], \tag{3a}$$

$$T_{\mathbf{k}}^{\mathrm{cub}} = -\beta \,\mathrm{Re}\left[\sum_{\mathbf{p},\mathbf{q}} D_{ij}(\mathbf{k}) \langle v^i_{-\mathbf{k}} v^l_{\mathbf{k}-\mathbf{p}-\mathbf{q}} v^l_{\mathbf{q}} v^j_{\mathbf{p}} \rangle\right], \tag{3b}$$

where we have employed sum convention for cartesian indices, $D_{ij}(\mathbf{k}) := \delta_{ij} - k_i k_j/k^2$ are the components of the projection tensor, $M_{njl}(\mathbf{k}) := -(\mathrm{i}/2)\,(k_j D_{nl}(\mathbf{k}) + k_l D_{nj}(\mathbf{k}))$, and we

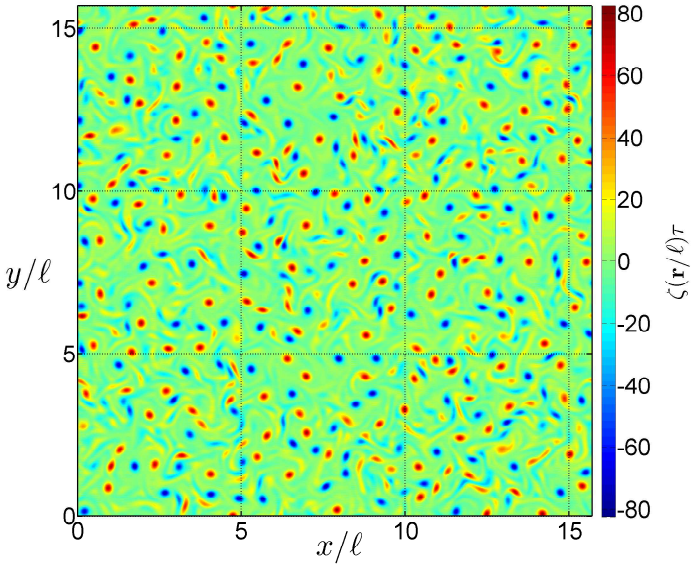

Figure 1: Snapshot of the two-dimensional vorticity field $\zeta = \partial_x v_y - \partial_y v_x$ right after the onset of the turbulent regime as obtained from a numerical solution of Eq.(1) using a pseudo-spectral code. The computation has been performed with 1024 (effective) points in each direction under the constraint of periodic boundary conditions. The Ekman parameter equals $\alpha\tau = -1$, implying that there are two energy sources acting at large scales - the two positive terms in the expression for $\gamma(k)$. The strength of the cubic nonlinearity is set to $\beta\tau v_0 = 0.5$ and for the advective term we have used $\lambda_0 = 3.5$. One can clearly see the highly disordered distribution of vortices justifying the classification of the regime as turbulent.

have omitted all time arguments for simplicity. The *Ekman term* (proportional to α) either injects ($\alpha < 0$) or dissipates ($\alpha > 0$) energy into/from the system with the corresponding rate being proportional to $E_{\mathbf{k}}$. Similarly, the remaining linear terms are also responsible for either local energy injection (Γ_0-term) or dissipation (Γ_2-term). The feature making the dynamics highly nontrivial are the nonlinear terms resulting from the advection term and the cubic nonlinearity in Eq. (1). They couple different wave numbers and provide a flow of energy in spectral space that (on average) balances the local injection or dissipation. The different terms in Eq. (2), as obtained from a numerical solution of Eq. (1) using a pseudo-spectral code, are shown in Fig. 2. Here, we have averaged over nearly 10 000 time steps and (employing spherical symmetry) summed over modes with the same absolute value (hence the scalar form of the index k). A distinctive feature of the *advective nonlinearity* (green curve) is that it is positive for small k but negative for intermediate k, and thus transports energy from large to small length scales. This inverse energy flow is well known for two-dimensional turbulent settings and can be attributed to the constraint of enstrophy conservation.[35] In the present context, it takes energy from the intermediate wave numbers where the Γ_0-injection (magenta) is particularly active and transports it to larger scales where it acts as an energy source together with the Ekman term (red) for $\alpha < 0$. At large length scales, those two sources are balanced by the cubic nonlinearity (dark blue) which acts as an energy sink for most wave numbers. This energy sink, however, has a nonlinear character which allows it to dynamically adjust its magnitude to the sources for a balance to be reached. Another important feature

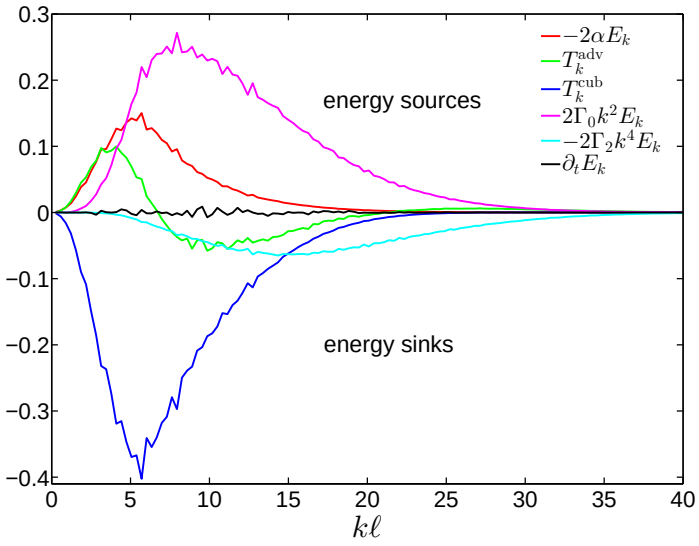

Figure 2: Spectral form of the different terms in Eq. (2) in the statistically stationary state (time averaged): red - Ekman term; green - advective nonlinearity T_k^{adv}; dark blue - cubic interaction T_k^{cub}; magenta - k^2-injection; light blue - k^4-dissipation; black - time average of the left-hand side. A positive contribution means that at these wave numbers the corresponding term acts as an energy source, and a negative value indicates an energy sink. One sees that the nonlinear terms change their character depending on the scale under consideration. At large and intermediate scales, however, the cubic nonlinearity is always dissipative. Additionally, the Ekman term can provide energy injection or dissipation depending on the sign of α. For the simulation presented here the latter was set to $\alpha\tau = -1$, i.e., it represents an additional energy source.

of the cubic interaction is that (at large scales) its contribution to the energy flow is roughly proportional to the energy spectrum E_k. Later in this work we will show that those two features of the cubic nonlinearity can be derived from a closure approximation for small k.

2.2 Spectral shell decomposition

To further assess the energy transfer among different length scales, we divide the spectral space into circular shells S_J, $J = 1, 2, 3, ...$ centered at $\mathbf{k} = 0$ such that the set $S_J = \{\mathbf{k} | k \in [k_{J-1}, k_J)\}$ fully covers the spectral space. The choice of the boundaries of the shells is specified in Section S.2 in the Supplemental Material. Moreover, we introduce the projection operator P_J defined as

$$(P_J f)(\mathbf{r}) := \langle f(\mathbf{r}) \rangle_J := \sum_{\mathbf{k} \in S_J} f_{\mathbf{k}} \mathrm{e}^{\mathrm{i}\mathbf{k}\cdot\mathbf{r}}. \tag{4}$$

Such a decomposition of the spectral space provides a useful mean for analyzing the nonlinear terms. The latter represent, in general, interactions between different spatial scales and computing the contributions arising from different shells will help us gain physical insight into those interactions, e.g., we can determine the degree of locality of the energy transfer due to the Navier-Stokes nonlinearity. Additionally, examining the symmetry of the shell-to-shell

coupling corresponding to the quadratic and cubic nonlinearity will reveal their completely different physical character.

Applying P_J on Eq. (1) leads to an evolution equation for the energy $E_J := \int |\langle \mathbf{v} \rangle_J|^2 \mathrm{d}\Omega/(2V)$ of shell S_J which reads

$$\frac{\partial E_J}{\partial t} = \sum_{\mathbf{k} \in S_J} \gamma(k) \, |\mathbf{v}_\mathbf{k}|^2 + \sum_I \Big(T_{IJ}^{\mathrm{adv}} + T_{IJ}^{\mathrm{cub}} \Big), \tag{5}$$

with the advective and cubic nonlinear terms

$$T_{IJ}^{\mathrm{adv}} = -\lambda_0 \sum_{\mathbf{k}} \overline{\langle \mathbf{v}_\mathbf{k} \rangle_J} \cdot \mathcal{F}\{(\mathbf{v} \cdot \nabla) \langle \mathbf{v} \rangle_I\}(\mathbf{k}) \, , \tag{6a}$$

$$T_{IJ}^{\mathrm{cub}} = -\beta \sum_{\mathbf{k}} \overline{\langle \mathbf{v}_\mathbf{k} \rangle_J} \cdot \mathcal{F}\{|\mathbf{v}|^2 \langle \mathbf{v} \rangle_I\}(\mathbf{k}) \, , \tag{6b}$$

where $\mathcal{F}$ denotes the Fourier transform as defined in Section S.1 in the Supplemental Material. Eqs. (6a) and (6b) represent an equivalent formulation of Eqs. **[S15a]** and **[S15b]** in terms of Fourier modes. Details of the derivation of the above spectral shell decomposition are presented in Section S.2 of the Supplemental Material.

The terms T_{IJ}^{adv} and T_{IJ}^{cub} characterize the transfer of energy between shells S_I and S_J. Due to the incompressibility constraint, T_{IJ}^{adv} is antisymmetric with respect to the shell indices I and J (see Section S.2 in the Supplemental Material), which implies that summing over both indices gives zero. This shows that (in an incompressible system) the Navier-Stokes nonlinearity neither injects nor dissipates energy but only redistributes it among the different shells S_J. T_{IJ}^{adv}, as obtained in numerical computations, is shown in Fig. 3 (a). In addition to verifying the antisymmetry, this also illustrates the direction of energy transfer in spectral space. There is a combination of forward and inverse energy flows. At intermediate wave numbers, there is mainly a forward energy cascade which is local in spectral space; see the areas next to the diagonal in Fig. 3 (a), where, red above the diagonal and blue below it indicate a flow from lower to larger wave numbers. Additionally, there is also a nonlocal inverse energy flow dominating at small wave numbers, represented by the smaller side branches in Fig. 3 (a). An additional way to view the energy transfer induced by the advective term is illustrated by the green curve in Fig. 2. In represents the cumulative effect of the two-dimensional structures seen in Fig. 3 (a). The Navier-Stokes nonlinearity extracts energy from the intermediate wave numbers (negative contribution) and supplies it to both smaller (inverse cascade) and larger (forward cascade) wave numbers. The contribution of the cubic nonlinearity, on the other hand, is symmetric ($T_{IJ}^{\mathrm{cub}} = T_{JI}^{\mathrm{cub}}$) and, therefore, cannot be viewed as a term which simply transfers energy from one shell to another in a conservative manner (see Section S.2 in the Supplemental Material). Since every second-rank tensor can be uniquely decomposed into a symmetric and an antisymmetric part, T_{IJ}^{cub} represents physical processes which are fundamentally distinct from a Navier-Stokes-like energy transfer. It does not redistribute energy between different shells. Instead, it couples different shells, say S_I and S_J, in such a way that the same amount of energy is either produced in both shells or extracted from them. The numerical results displayed in Fig. 3 (b) clearly show that the entries of T_{IJ}^{cub} are dominated by the diagonal terms while the off-diagonal terms are negligibly small. Note that the curve in the inset resembles closely the blue line in Fig. 2. Moreover, the diagonal entries are negative indicating the dissipative nature of the cubic nonlinearity. This feature together

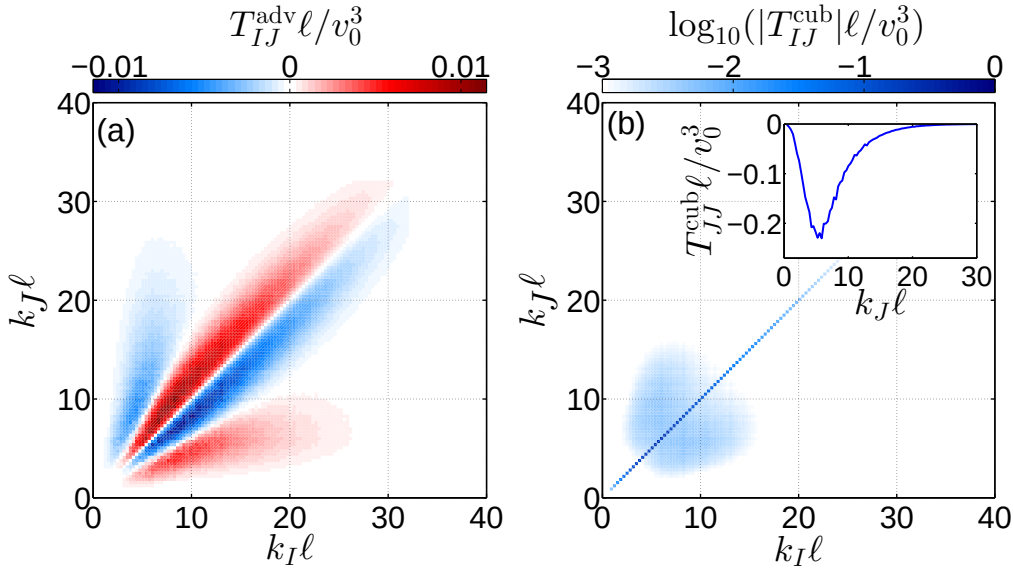

Figure 3: Numerical computation of the shell-to-shell couplings $T^{\rm adv}_{IJ}$ and $T^{\rm cub}_{IJ}$ as given in Eqs. (6); all shells have the same width of three times the minimal wave number Δk and a time average over the statistically stationary state has been performed. (a) The coupling term $T^{\rm adv}_{IJ}$ due to the advective Navier-Stokes nonlinearity in units of v_0^3/ℓ. It exhibits both forward and backward energy flow in spectral space. At intermediate and large wave numbers there is a local forward flux; see the lobes close to the diagonal. In contrast, for small k, there is an inverse flux nonlocal in spectral space; see the side branches. (b) The coupling term $T^{\rm cub}_{IJ}$ due to the cubic nonlinearity in units of v_0^3/ℓ; note the logarithmic scale. In contrast to the Navier-Stokes term, $T^{\rm cub}_{IJ}$ is symmetric in the shell indices. In addition, it is almost diagonal indicating that coupling between different shells is negligible. This shows that at large scales the cubic interaction can be well approximated as a local dissipation term. Inset displays only the diagonal entries on a linear scale.

with the different physical interpretation of the cubic term represent the central results that the shell-to-shell decomposition yields. Both aspects are essential for the cubic interaction and should be captured by a successful closure approximation.

2.3 Cubic damping term

To make progress beyond a numerical analysis, we next seek an approximate solution for the time evolution of the energy spectrum and the ensuing stationary state. The analysis is complicated by the fact that the right hand side of Eq. (2) involves third and fourth order velocity correlation functions, $T^{\rm adv}_{\mathbf{k}}$ and $T^{\rm cub}_{\mathbf{k}}$. Formulating evolution equations for those gives rise to even higher-order velocity correlations on the right-hand side. One way to deal with this 'hierarchy' problem is to make approximations at some level (via a 'closure relation'), leading to a closed set of equations. Guided by the observation that the statistics of the velocity field at large spatial separations in classical two-dimensional Navier-Stokes turbulence is very close to Gaussian (which we also confirmed numerically for Eq. (1) as explained in Section S.3 in the Supplementary Material), a natural way to approach the cubic damping term in Eq. (2) is via

the quasi-normal approximation [31], also known as Millionshchikov hypothesis.[36] According to this idea, third-order correlations, e.g., $\langle v^i_{-\mathbf{k}} v^l_{\mathbf{k}-\mathbf{p}} v^j_{\mathbf{p}} \rangle$, are non-zero, in contrast to a purely normal distribution, but the even-order correlations are approximately sums of products of all possible combinations of second-order correlations (as in Wick's theorem). Introducing the scalar correlation function $Q_k(t)$ defined via the relation $D_{ij}(\mathbf{k})Q_k(t) := \langle v^i_{-\mathbf{k}}(t) v^j_{\mathbf{k}}(t) \rangle$ and employing homogeneity and isotropy of space, one arrives (for a two-dimensional setting) at

$$T^{\mathrm{cub}}_{\mathbf{k}} \approx -\beta Q_k \sum_{\mathbf{p}} \left(2\frac{(\mathbf{k}\cdot\mathbf{p})^2}{k^2 p^2} + 1 \right) Q_p \approx -8\beta\, E_{tot}\, E_k, \tag{7}$$

where E_{tot} denotes the total energy of the system; for details of the derivation see Section S.3 in the Supplemental Material. Hence, the cubic damping term in Eq. (2) can be approximated by an expression that is directly proportional to the energy spectrum E_k. This resonates with the information provided by Fig. 3 (b), namely that the diagonal terms are the dominant ones in T^{cub}_{IJ}. In other words, the cubic damping term is of the same form as the linear Ekman damping, however with the important difference that the corresponding damping rate is not constant but proportional to the total energy E_{tot} of the system. This captures the nonlinear character of the cubic damping term: It provides a dynamical response of the system at large spatial scales, where an increase of the total energy of the system will lead to a stronger dissipation which, in turn, will decrease E_k. This nonlinear feature helps to maintain the spectral energy balance and achieve a statistically stationary state. The latter cannot always be attained if $\beta = 0$. Our investigations revealed that in this case there is a critical value for α (necessarily positive) below which the dissipation due to friction is insufficient and cannot balance the energy that accumulates at the large scales as a result of the inverse energy flow in two-dimensional Navier-Stokes systems.

2.4 Advective nonlinearity

In contrast to the cubic damping term, the advective nonlinearity in Eq. (2) produces an expression that involves third-order correlations. Thus, one cannot directly apply the quasi-normal approximation to it. One way to tackle this problem would be to use the exact equation of motion and obtain from it an evolution equation for the third-order correlation in analogy to the procedure leading to Eq. (2). On the right-hand side of such an equation, the advective nonlinearity will result in a fourth-order correlation for which the quasi-normal approximation is applicable. However, the exact equation of motion contains also a cubic term. In the evolution equation for the third-order correlation this term will give rise to a fifth-order correlation which cannot be directly treated with the quasi-normal approximation. This hierarchical scheme can, nevertheless, lead to a closed system of equations after applying the Millionshchikov hypothesis, but due to the cubic nonlinearity in Eq. (1) the resulting system of equations is highly complicated and tractable only numerically.
Since our goal here is to arrive at an analytical approximation for the energy spectrum at small wave numbers, we choose a more heuristic approach. As already discussed, the advective nonlinearity only redistributes energy among the different modes. This implies an energy flux in spectral space, defined as $\Pi^{\mathrm{adv}}_k = -\int_0^k T^{\mathrm{adv}}_p \mathrm{d}p$, which is taken to be proportional to the energy E_k at any given scale. The energy corresponding to an eddy of size $\sim 1/k$ scales as $k\,E_k$, which suggest the relation

$$\Pi^{\mathrm{adv}}_k \propto \omega_k\, k\, E_k, \tag{8}$$

where ω_k is a characteristic frequency which may vary with k. Since ω_k is still undetermined, the above relation merely shifts the challenge to finding the function ω_k. However, it suggests a physical interpretation for it. In two- and three-dimensional Navier-Stokes turbulence this frequency is determined by $\omega_k^2 \sim \int_0^k p^2 E_p \mathrm{d}p$. [37] The physical picture behind this relation is that $1/\omega_k$ can be viewed as the characteristic distortion time at length scale $1/k$. For the energy cascade in classical turbulence ω_k scales as $k^{2/3}$. Thus, with respect to a given scale $1/k$, larger eddies have longer eddy-turn-over times while smaller eddies have shorter ones. This implies that over a time period of the order of the eddy-turn-over time at scale $1/k$ the effects of the larger wave numbers average out due to their faster dynamics. On the other hand, the comparatively slower dynamics of the larger length scales (compared to $1/k$) indicate that they will provide a coherent contribution to the average shear rate acting at the scale $1/k$. Given the decrease of E_k with k in the cascade range of Navier-Stokes turbulence, the main contribution to the integral comes from the part of the integrand around $p \sim k$. Thus, most of the shear stems from wave numbers of a magnitude similar to k which relates to the locality of the classical energy cascade. Eq. (8) together with the integral expression for ω_k given above simplify the equations and provide a closure which, in the limit of an energy/enstrophy cascade, i.e., constant energy/enstrophy flux, yields the Kraichnan solution for the energy spectrum in the energy/enstrophy inertial range [37]. As is evident in Fig. 2, however, at large scales there is no range of wave numbers for which the advective nonlinearity is zero, i.e., there is no inertial range. Furthermore, as shown in Fig. 4, the spectral form

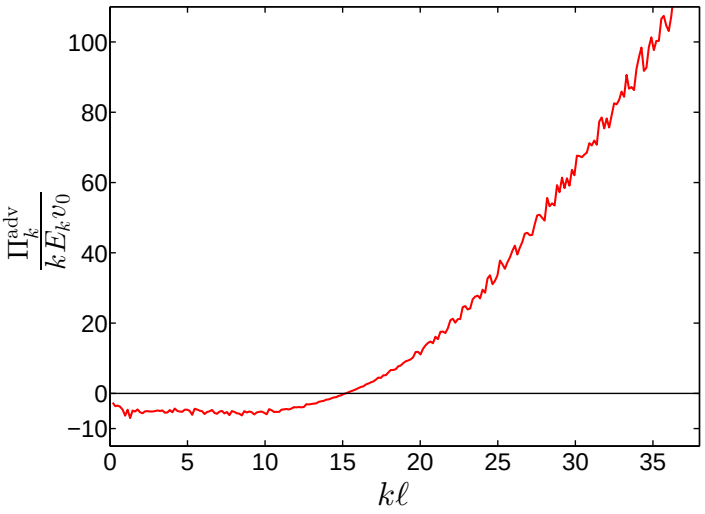

Figure 4: Numerical computation of the frequency ω_k as a function of k as defined by Eq. (8). Owing to the positive definiteness of the denominator kE_k, the sign of the function agrees with the sign of the energy flux arising from the advective nonlinearity. Thus, there is evidently an inverse energy flow (negative flux) at large length scales and a forward energy flow (positive flux) at small length scales. Additionally, ω_k is approximately constant at small wave numbers. The numerical simulation was performed with $\alpha\tau = 1$.

of the ratio $\Pi_k^{\mathrm{adv}}/(kE_k)$ is constant at large scales, i.e., $\omega_k = \omega_c = \mathrm{const}$, implying that the physics in our case is qualitatively different from what we have in classical Navier-Stokes turbulence, both two- and three-dimensional. The result that the characteristic frequency is

not a function of the local wave number but instead a constant over a wide range in spectral space implies a kind of synchronization of the large-scale structures. Such a synchronization deviates considerably from the classical $\omega_k \propto k^{2/3}$ scaling and requires nonlocal interactions involved in the inverse energy cascade at small k as seen in Fig. 3 (a). In addition, in classical turbulence models large spatial scales are more energetic than smaller ones giving the former the potential to shear and distort the latter. For Eq. (1), however, the energy spectrum E_k first increases with k up to some maximum and then decreases again; see the red curve in Fig. 2. Hence, for the spectral region we are interested in, the larger scales are not able shear the smaller ones. In summary, our investigation of the advective nonlinearity in this model shows that at small wave numbers there is a distinct constant frequency ω_c which controls the energy transfer at large scales. Incorporating this insight into our analysis will provide us with an approximate solution for the energy spectrum at those scales.

2.5 Variable spectral exponent

In the statistically stationary state, time-averaging Eq. (2) will give zero on the left-hand side, which yields

$$-2\Big(\alpha + 4\beta E_{tot} + \Gamma_0 k^2 - \Gamma_2 k^4\Big) E_k - \frac{\mathrm{d}\Pi_k^{\mathrm{adv}}}{\mathrm{d}k} = 0, \tag{9}$$

where we have already incorporated the result of the quasi-normal approximation for the cubic damping term. Discarding the term proportional to Γ_2 which is negligible at small wave numbers and using Eq. (8) with constant ω_k one arrives at a differential equation for the energy spectrum E_k the solution of which reads

$$E_k = \widetilde{E}_0 k^\delta \exp\left(-\frac{\Gamma_0}{\lambda_0 \omega_c} k^2\right), \tag{10}$$

where $\widetilde{E}_0$ is a constant of integration and the exponent is given by $\delta = (2\alpha + 8\beta E_{tot})/(\lambda_0 \omega_c) - 1$. Eq. (10) shows that at small wave numbers ($k \to 0$) the energy spectrum behaves as a power law. However, the exponent δ of this power law is not universal but depends (directly and indirectly) on various system parameters. Qualitatively, a stronger dissipation, i.e., a positive α and a higher factor of βE_{tot}, will induce a steeper power law. An example is shown in Fig. 5 where the numerical solution of Eq. (1) is presented for two different values of α. In both cases, the system exhibits clear power law spectra over more than one order of magnitude in wave number space, and it is evident that our model predicts the correct qualitative dependence of the spectral exponents. A quantitative test of our semi-analytical result can be undertaken by carrying out numerical simulations for different values of α. We note in passing that such a parameter scan requires that there are always enough instabilities to drive the turbulence, and that statistical homogeneity and isotropy are ensured. The linear growth rate of the most unstable mode equals $-\alpha + \Gamma_0^2/(4\Gamma_2)$, which gives an upper bound on the variation of α once Γ_0 and Γ_2 have been set. On the other hand, the term $-\alpha \mathbf{v}$ in Eq. (1) tries to destroy the statistical isotropy of the system. Thus, the energy injected by the α-term must be considerably smaller than that injected by the Γ_2-term, which imposes a lower bound on α. The result from such a parameter scan of the numerical solution of Eq. (1) is displayed in Fig. 6 where every point is obtained by fitting a power law on the left end of the energy spectrum. The data from our investigation show a linear dependence of the slope δ on the parameter α which agrees with the expression for δ provided by our model. Further

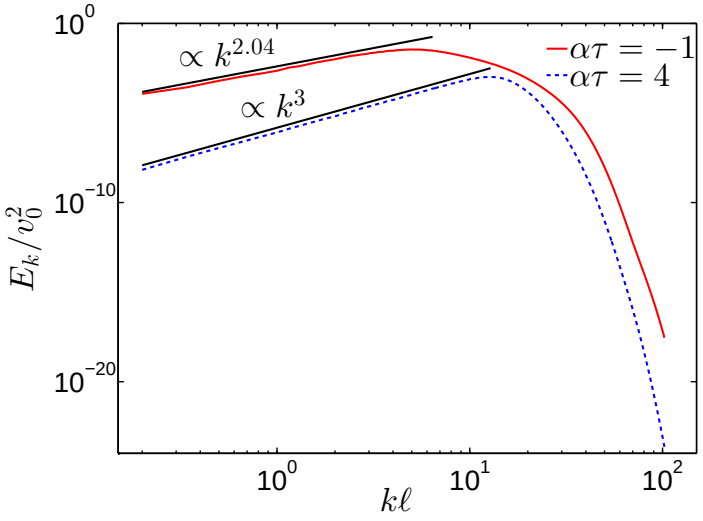

Figure 5: Time-averaged energy spectrum E_k for two different values of $\alpha\tau$ at the two ends of the parameter domain supporting the turbulent regime, $\alpha\tau = -1$ and $\alpha\tau = 4$. There is a clear power law at large scales and the effect of varying the strength of the Ekman term manifests as a variation of its slope. In general, more intensive energy injection (via the parameter α) leads to a less steeper slope of the power law, more energy at each scale and a peak of the energy spectrum that occurs at smaller wave numbers.

numerical simulations indicate that the dependence of the slope on the strength of the cubic interaction β is qualitatively the same but quantitatively much weaker. This can be due to the factor βE_{tot} appearing in δ. Stability analysis shows that for $\lambda_0 = \Gamma_0 = \Gamma_2 = 0$ and $\alpha < 0$ an ordered state arises with a constant velocity field and total system energy $E_{tot} \propto 1/\beta$. If a similar scaling applies also in the presence of the advective nonlinearity and the other linear terms, then the product βE_{tot} should exhibit only weak dependence on β.

3 Conclusion

In the present work, we have investigated the properties of a continuum model describing the turbulent motion of active fluids, e.g., dense bacterial suspensions, driven by internal instabilities. While turbulence in conventional fluids is generally associated with a substantial scale separation between the drive and dissipation range and by the presence of a conservative energy/enstrophy cascade throughout an inertial range, active systems display turbulent behavior and power-law spectra even when those conditions are not met. In addition to the convective nonlinearity of Navier-Stokes type, the model contains a novel cubic interaction, which is not energy-conserving. Analytical and numerical considerations revealed that at large scales, it behaves like an Ekman damping with a frequency that is set by the system self-consistently. Furthermore, our analysis suggests that the conventional view on turbulence might not be applicable to active fluids since there the scales of turbulent motion are not governed entirely by the nonlinear terms. Instead, the energy spectrum arises from the balance of several terms, some of which are linear. As a consequence and in contrast to conventional Navier-Stokes turbulence, the steepness of the energy spectrum is not universal but depends

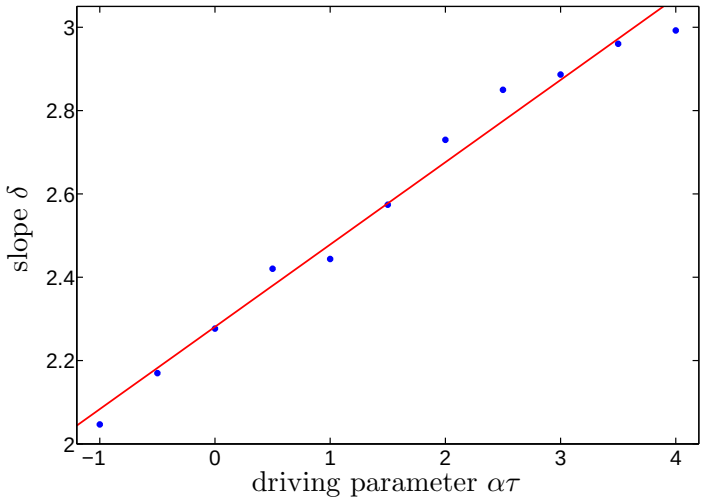

Figure 6: Variation of the slope of the energy spectrum at small wave numbers with respect to α. The steepness of the power law at large scales varies continuously with the driving parameter in a nearly linear fashion as long as there is a statistically isotropic turbulent regime. The parameter range where this applies derives from the condition that there are enough linear instabilities to sustain the turbulence, i.e., α should not be too large, and the energy injection from the Ekman term should not dominate over the Γ_0-term, i.e., α should not be too negative.

on system parameters. These properties should be observable in laboratory experiments and also apply to other active fluids. Overall, one can argue that the high-dimensional nonlinear dynamics in such systems defines a new class of turbulence, involving a high degree of self-organization, which is distinct from the Navier-Stokes case.

Acknowledgements

V. B. would like to thank A. Bañón Navarro, M. Oberparleiter and D. Groselj for helpful discussions. The research leading to these results has received funding from the European Research Council under the European Unions Seventh Framework Programme (FP7/2007-2013)/ERC Grant Agreement No. 277870. It was also supported by the German Excellence Initiative via the program 'NanoSystems Initiative Munich' (NIM) and the Deutsche Forschungsgemeinschaft (DFG) in the context of SFB 863 "Forces in Biomolecular Systems" (Project B02).

References

[1] Haitao X *et al.* (2014) *Flight-crash events in turbulence. Proc Natl Acad Sci USA* 111:7558-7563

[2] Perlekar P, Benzi R, Clercx HJH, Nelson DR, Toschi F (2014) *Spinodal decomposition in homogeneous and isotropic turbulence. Phys Rev Lett* 112:014205

[3] Kolmogorov AN (1941) *The local structure of turbulence in incompressible viscous fluid for very large Reynolds number. Dokl Akad Nauk SSSR* 30:299-303

[4] Wensink HH *et al.* (2012) *Meso-scale turbulence in living fluids. Proc Natl Acad Sci USA* 109:14308-14313

[5] Sokolov A, Aranson IS (2012) *Physical properties of collective motion in suspensions of bacteria. Phys Rev Lett* 109:248109

[6] Zhou S, Sokolov A, Lavrentovich OD, and Aranson IS (2014) *Living liquid crystals. Proc Natl Acad Sci USA* 111:1265-1270

[7] Dombrowski C, Cisneros L, Chatkaew S, Goldstein RE, Kessler JO (2004) *Self-concentration and large-scale coherence in bacterial dynamics. Phys Rev Lett* 93:098103

[8] Thampi SP, Golestanian R, Yeomans JM (2013) *Velocity correlations in an active nematic. Phys Rev Lett* 111:118101

[9] Thampi SP, Golestanian R, Yeomans JM (2014) *Vorticity, defects and correlations in active turbulence. Phil Trans R Soc A* 372:2029

[10] Chen X, Dong X, Be'er A, Swinney HL, Zhang HP (2012) *Scale-invariant correlations in dynamic bacterial clusters. Phys Rev Lett* 108:148101

[11] Simha RA, Ramaswamy S (2002) *Hydrodynamic fluctuations and instabilities in ordered suspensions of self-propelled particles. Phys Rev Lett* 89:058101

[12] Thampi SP, Golestanian R, Yeomans JM (2014) *Active nematic materials with substrate friction. Phys Rev E* 90:062307

[13] Stresing R, Peinke J, Seoud RE, Vassilicos JC (2010) *Defining a new class of turbulent flows. Phys Rev Lett* 104:194501

[14] Elmegreen BG, Scalo J (2004) *Interstellar turbulence I: Observations and processes.* Annu Rev Astron Astrophys 42:211-273

[15] Görler T, Jenko F (2008) *Scale separation between electron and ion thermal transport. Phys Rev Lett* 100:185002; *Multiscale features of density and frequency spectra from nonlinear gyrokinetics. Phys Plasmas* 15:102508

[16] Bratanov V, Jenko F, Hatch DR, Wilczek M (2013) *Nonuniversal power-law spectra in turbulent systems. Phys Rev Lett* 111:075001

[17] Dunkel J, Heidenreich S, Bär M, Goldstein RE (2013) *Minimal continuum theories of structure formation in dense active fluids.* New J Phys 15:045016

[18] Dunkel J *et al.* (2013) *Fluid dynamics of bacterial turbulence. Phys Rev Lett* 110:228102

[19] LaQuey RE, Mahajan SM, Rutherford PH, Tang WM (1975) *Nonlinear saturation of the trapped-ion mode. Phys Rev Lett* 34:391-394

[20] Cohen BI, Krommes JA, Tang WM, and Rosenbluth MN (1976) *Non-linear saturation of the dissipative trapped-ion mode by mode coupling . Nucl Fusion* 16:971-992

[21] Kuramoto Y, Tsusuki T (1974) *Reductive perturbation approach to chemical instabilities. Prog Theor Phys* 52:1399-1401

[22] Kuramoto Y (1978) *Diffusion-induced chaos in reaction systems. Prog Theor Phys Suppl* 64:346-367

[23] Sivashinsky GI (1977) *Nonlinear analysis of hydrodynamic instability in laminar flames-I. Derivation of basic equations. Acta Astron* 4:1177-1206; (1979) *On self-turbulization of a laminar flame. Acta Astron* 6:569-591

[24] Shraiman BI (1986) *Order, disorder, and phase turbulence. Phys Rev Lett* 57:325-328

[25] Swift J, Hohenberg PC (1977) *Hydrodynamics fluctuations of the convective instability. Phys Rev A* 15:319-328

[26] Sain A, Manu, Pandit R (1998) *Turbulence and multiscaling in the randomly forced Navier-Stokes equation. Phys Rev Lett* 81:4377-4380

[27] Biferale L, Lanotte AS, Toschi F (2004) *Effects of forcing in three-dimensional turbulent flows. Phys Rev Lett* 92:094503

[28] Toner J, Tu Y, Ramaswamy S (2005) *Hydrodynamics and phases of flocks. Ann Phys* 318:170-244

[29] Toner J, Tu Y (1998) *Flocks, herds and school: A quantitative theory of flocking. Phys Rev E* 58:4828-4858

[30] Marchetti MC *et al.* (2013) *Hydrodynamics of soft active matter. Rev Mod Phys* 85:1143-1189

[31] Monin AS, Yaglom AM (1975) *Statistical fluid mechanics.* (MIT Press, Cambridge, Mass.)

[32] Gioia G, Chakraborty P (2006) *Turbulent friction in rough pipes and the energy spectrum of the phenomenological theory. Phys Rev Lett* 96:044502

[33] Tran T *et al.* (2010) *Macroscopic effects of the spectral structure in turbulent flows. Nat Commun* 6:438-441

[34] Kraichnan RH (1967) *Inertial ranges in two-dimensional turbulence. Phys Fluids* 10:1417-1423

[35] Fjørtoft R (1953) *On the changes in the spectral distribution of kinetic energy for two-dimensional, non-divergent flow. Tellus* 5:225-230

[36] Millionshchikov MD (1941) *Theory of homogeneous isotropic turbulence. Dokl Akad Nauk SSSR* 32:611-614

[37] Kraichnan RH (1971) *Inertial-range transfer in two- and three-dimensional turbulence. J Fluid Mech* 47:525-535

Supplementary Information: Self-organization in active fluids

V. Bratanov[1], F. Jenko[2] and E. Frey[3]

[1]Max Planck Institute for Plasma Physics, Boltzmannstr. 2, 85748 Garching, Germany
[2]Department of Physics and Astronomy, University of California, Los Angeles, California 90095, USA
[3]Arnold Sommerfeld Center for Theoretical Physics and Center for NanoScience, Department of Physics, Ludwig-Maximilians-Universität München, Theresienstr. 37, 80333 München, Germany

S.1 Normalization and numerical methods

Normalization. For the sake of completeness, we discuss here briefly the normalization of the quantities used, and describe the numerical implementation of the continuum model. Written in dimensional units, Eq. (1) reads

$$\frac{\partial \mathbf{v}}{\partial t} + \lambda_0(\mathbf{v}\cdot\nabla)\mathbf{v} = -\frac{1}{\rho}\nabla p - (\alpha + \beta|\mathbf{v}|^2)\mathbf{v} - \Gamma_0\Delta\mathbf{v} - \Gamma_2\Delta^2\mathbf{v}, \tag{S1}$$

where ρ denotes density of the fluid and shall be considered constant. In contrast to Ref. [1], we have omitted the term $\lambda_1\nabla|\mathbf{v}|^2$ since, for constant λ_1, it is obsolete. Being a gradient of a scalar function, it is of the same type as the pressure term and can be absorbed in it. Additionally, our definition for Γ_0 is such that positive values correspond to linear instabilities. Due to the nature of the problem, we only need to specify a velocity and a length scale, v_0 and ℓ respectively, with the resulting time scale being $\tau = \ell/v_0$. The parameters Γ_0 and Γ_2 controlling the linear instability and dissipation give rise to a velocity scale defined as $v_0 = \sqrt{\Gamma_0^3/\Gamma_2}$. For the determination of the length scale, we consider the linear growth rate γ of the spectral modes given by $\gamma(k) = -\alpha + \Gamma_0 k^2 - \Gamma_2 k^4$. It has a maximum located at $k_{\max} = \sqrt{\Gamma_0/(2\Gamma_2)}$ after which it decreases and eventually becomes negative, meaning that the short wavelength modes are linearly stable. Thus, the linear instability is most prominent at the spatial scale of $\pi/k_{\max}$. Proper resolution of the physical processes involved demands that the size of the system is much larger than $\pi/k_{\max}$. Hence, we define our normalization length scale as $\ell = 5\pi/k_{\max} = 5\pi\sqrt{2\Gamma_2/\Gamma_0}$. The physical quantities and operators map to their dimensionless forms as

$$v \to v v_0 \; ; \; t \to t\tau \; ; \; p \to p v_0^2 \rho \; ; \; \alpha \to \alpha/\tau \; ; \tag{S2}$$

$$\beta \to \frac{\beta}{\ell v_0} \; ; \; \Gamma_0 \to \Gamma_0 \ell v_0 \; ; \; \Gamma_2 \to \Gamma_2 \ell^3 v_0 \text{ and } \nabla \to \frac{1}{\ell}\nabla. \tag{S3}$$

Using the velocities and length scales defined above sets the normalized values of the parameters Γ_0 and Γ_2 as $\Gamma_0 = 1/(5\sqrt{2}\pi) \approx 0.045$ and $\Gamma_2 = \Gamma_0^3 \approx 9 \cdot 10^{-5}$. The normalization units

chosen above are the same as those used in Ref. [1] which facilitates comparison. All the numerical results presented here were obtained with $\lambda_0 = 3.5$ and a normalized value for β of $\beta = 0.5$. Given that $\alpha = -1$ and the different sign convention for Γ_0, the parameters used in this paper correspond to the experimental values characterizing the bacterial suspension described in Ref. [1].

Eq. (1) possesses five different parameters which makes a thorough investigation of its complete parameter space a very tedious task. In order to bring some structure into this highly dimensional parameter space, we present some limit cases in the table below. It is important to note that for $\beta < 0$ the dynamics represented by Eq. (1) does not reach a stationary state and the kinetic energy of the velocity field grows without a limit. Thus, this case is of no physical relevance.

	λ_0	α	β	Γ_0	Γ_2	limit case
1.	1	0	0	$\Gamma_0 < 0$	0	Classical Navier-Stokes equation
2.	1	0	0	0	$\Gamma_2 > 0$	Navier-Stokes equation with hyperviscosity of the second order
3.	1	$\alpha > 0$	0	$\Gamma_0 < 0$	0	Navier-Stokes equation with large-scale friction, i.e., Ekman damping
4.	1	0	0	$\Gamma_0 > 0$	$\Gamma_2 > 0$	Straightforward multi-dimensional generalization of the Kuramoto-Sivashinsky equation for incompressible velocity fields

Table 1: Classification of the different limit cases for Eq. (1) depending on the choice of parameters.

Numerical methods. Numerical solutions of Eq. (1) have been obtained via the pseudo-spectral approach [2], which is common in Computational Fluid Dynamics. According to it spatial derivatives are computed in Fourier space where they reduce to simple multiplication. The nonlinear terms, on the other hand, are computed in real space since they correspond to a convolution in Fourier space which is a computationally expensive procedure. Thus, the pseudo-spectral approach relies heavily on the fast Fourier transform algorithms as the one developed by Cooley and Tukey.[3] (Cooley and Tukey actually independently rediscovered an algorithm that has been known before with the earliest records dating back to a work of Gauss.[4]) The time evolution is computed numerically by the exponential time differencing scheme first developed in Ref. [5] and later improved in Ref. [6] where a fourth-order Runge-Kutta method has been employed. The underdetermined system of equations (1) is completed by the incompressibility condition $\nabla \cdot \mathbf{v} = 0$ and solved on the quadratic domain $[0, L_x] \times [0, L_y]$ with $L_x = L_y = L$ and periodic boundary conditions. The decomposition in Fourier series is achieved as

$$\mathbf{v}(\mathbf{r}, t) = \sum_{\mathbf{k}} \mathbf{v}_{\mathbf{k}}(t) \mathrm{e}^{\mathrm{i}\mathbf{k}\cdot\mathbf{r}}, \tag{S4}$$

where the components of the wave number vector $\mathbf{k} = (k_x, k_y)$ are related to the system size by $k_{x,y} = n2\pi/L_{x,y}$ with $n \in \mathbb{Z}_0$. For the ease of notation we omit the traditional $\widehat{\ }$ symbol. It should be clear from the corresponding argument if we mean the real-space function or

the Fourier component. According to the definition given above, the Fourier coefficients are determined as

$$\mathbf{v}_{\mathbf{k}}(t) = \frac{1}{L_x L_y} \int_0^{L_y} \int_0^{L_x} \mathbf{v}(\mathbf{r}, t) \mathrm{e}^{-\mathrm{i}\mathbf{k}\cdot\mathbf{r}} \mathrm{d}x\mathrm{d}y =: \mathcal{F}\{\mathbf{v}\}(\mathbf{k}, t), \tag{S5}$$

where the real-space coordinate vector is given by $\mathbf{r} = (x, y)$. Note that the pseudo-spectral approach introduces the so-called aliasing errors when computing the nonlinear term. In order to avoid that in numerical simulations of Navier-Stokes flows, one uses the 3/2 dealiasing rule. It consists in neglecting the higher 1/3 of the Fourier modes, i.e., the 'effective' Fourier modes are only 2/3 of the numerical ones. However, such a 3/2 rule can be applied only in the case of quadratic nonlinearities. For a cubic nonlinearity as in Eq. (1) the 3/2 dealiasing rule, standard in Navier-Stokes simulations, is insufficient. Instead, one should set to zero the upper half of the Fourier components.[7]

The solution of Eq. (1) in the part of parameter space we are interested in exhibits rapid fluctuations as typical for turbulent systems. The same applies also for quantities like the energy of a given mode or the total energy of the system. In the turbulence literature one defines the so-called 'ensemble average' which corresponds to an average over many possible realizations of the flow due to different initial conditions. However, such an average procedure is computationally extremely demanding. In the case of a system that reaches a statistically stationary regime one uses a time average instead, denoted by $\langle\cdot\rangle$, which is performed over a time window that starts after the onset of the statistically stationary state. In mathematical terms, for an arbitrary function $f(t)$ we have that

$$\langle f \rangle := \frac{1}{T} \int_{t_1}^{t_1+T} f(t) \mathrm{d}t. \tag{S6}$$

For a discrete time variable t the integral becomes a sum. Under the assumption of ergodicity the definition above yields the same result as an ensemble average.

In Ref. [1], where the continuous model we study here has been introduced, the main goal has been to compare its results with experimental measurements and with the findings based on more basic SPR (self-propelled rods) models. This determined the size of the real-space domain used in the simulations. In this article, however, we aim for a more fundamental examination of the turbulent dynamics produced by Eq. (1). Since we are interested in the spectral range at small wave numbers, we investigate the convergence of the numerical results when the box size becomes larger. The latter is inversely proportional to the smallest nonzero wave number we have, meaning that a larger real-space domain allows for a better representation of the small-k part of the energy spectrum. Numerical simulations of Eq. (1) for different domain sizes yield the energy spectra displayed in Fig. 1. The box size and number of points representing numerically the real-space domain that have been used for obtaining the red curve are nearly the same as those used in Ref. [1] and the slope of $k^{5/3}$ given by the upper black line is the one reported there. Due to the parameters of the simulation the smallest wave number is still rather large and close to the peak of the spectrum. Considering that there are only three points before the peak, it is hard to justify a power law in that region. Note that for obtaining an one-dimensional spectrum from a two-dimensional spectral representation one has to group together modes with similar $|\mathbf{k}|$. For the first few k-points

such a grouping can lead to notable ambiguity in the value of k assigned to the whole group and, thereby, influence the form of the curve. Therefore, the slope of a power law calculated by using only the first few points will be very sensitive to such numerical details. The blue curve, on the other hand, has been obtained with a much larger domain size and number of points (effectively 1024×1024 or 2048×2048 including dealiasing) and represents the simulation parameters used for all the numerical results reported here. It is evident that, in this case, there is a much larger (over one order of magnitude) domain at small k with a prominent power law of nearly $E(k) \propto k^2$ for this set of parameters (given by the lower black line) which, in addition, is also more robust. Thus, our analysis shows that the form of the power law

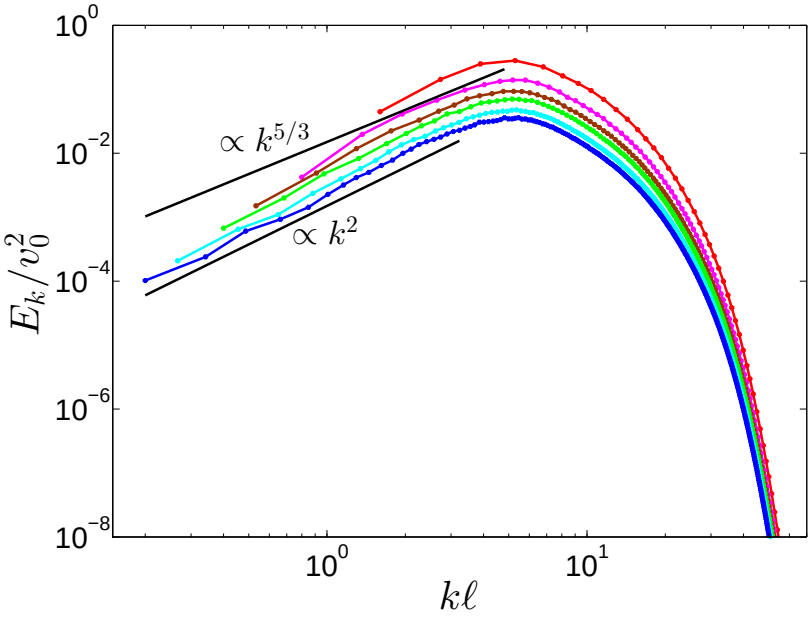

Figure 1: Numerical computation of the energy spectrum for different domain sizes: red - $\Omega = [0, 1.25\pi\ell] \times [0, 1.25\pi\ell]$; magenta - $\Omega = [0, 2.5\pi\ell] \times [0, 2.5\pi\ell]$; brown - $\Omega = [0, 3.75\pi\ell] \times [0, 3.75\pi\ell]$; green - $\Omega = [0, 5.0\pi\ell] \times [0, 5.0\pi\ell]$; cyan - $\Omega = [0, 7.5\pi\ell] \times [0, 7.5\pi\ell]$; blue - $\Omega = [0, 10.0\pi\ell] \times [0, 10.0\pi\ell]$. The numerical resolution was kept constant in all simulations. A rather large box size is needed for the manifestation of an unambiguous power law at small wave numbers. The numerical simulations were performed with $\alpha\tau = -1$.

is sensitive to finite-size effects of the simulation domain. With increasing the box size and keeping all physical parameters constant, it converges to a value that is different from the one presented in Ref. [1].

S.2 Symmetry of the nonlinear transfer terms

Generally speaking, nonlinear terms tend to play a key role in determining the behavior of complex systems. This is also true here. In the main part of the paper, these terms were studied quantitatively by introducing specific projection operators in spectral space as defined in Eq. (4). One can easily verify that P_J is idempotent and, thus, indeed a projection operator. In addition, P_J is self-adjoint with respect to the usual scalar product in $L^2(\Omega)$ and commutes

with temporal and spatial derivatives. This definition of P_J is still rather general and we have the freedom to choose the boundaries k_J of the individual shells. In the turbulence literature the shells are usually chosen such that $k_{J+1}/k_J = \text{const} > 1$. For analysing the spectral region of small wave numbers, however, this is rather inconvenient, since we want to have as many shells as possible in this spectral range. Thus, we construct the shells to be of equal width which will not change the results of our analysis. The numerical results reported in this work are obtained with the width of the circular bands being $3\Delta k$, where Δk is the difference between two adjacent modes along the x- or y-axis. This ensures that every shell contains an appreciable number of modes and thereby reduces statistical fluctuations.
Applying P_J on Eq. (1) gives us an evolution equation for the filtered velocity field $\langle \mathbf{v} \rangle_J$. Multiplying with $\langle \mathbf{v} \rangle_J$, integrating over space and taking into account that the energy of each spectral shell is given by $E_J = \int |\langle \mathbf{v} \rangle_J|^2 \mathrm{d}\Omega/(2V)$ we arrive at

$$\frac{\partial E_J}{\partial t} = -2\alpha E_J - \lambda_0 \frac{1}{V} \int_\Omega \langle \mathbf{v} \rangle_J \cdot \langle (\mathbf{v} \cdot \nabla)\mathbf{v} \rangle_J \mathrm{d}\Omega - \\ - \beta \frac{1}{V} \int_\Omega \langle \mathbf{v} \rangle_J \cdot \langle |\mathbf{v}|^2 \mathbf{v} \rangle_J \mathrm{d}\Omega - \Gamma_0 \frac{1}{V} \int_\Omega \langle \mathbf{v} \rangle_J \cdot \Delta \langle \mathbf{v} \rangle_J \mathrm{d}\Omega - \Gamma_2 \frac{1}{V} \int_\Omega \langle \mathbf{v} \rangle_J \cdot \Delta^2 \langle \mathbf{v} \rangle_J \mathrm{d}\Omega. \quad \text{(S7)}$$

Due to the periodic boundary conditions and the incompressibility constraint, the contribution of the pressure term vanishes , i.e.,

$$\int_\Omega \langle \mathbf{v} \rangle_J \cdot \nabla \langle p \rangle_J \mathrm{d}\Omega = \langle p \rangle_J \langle \mathbf{v} \rangle_J \cdot \mathrm{d}\boldsymbol{\sigma} \Big|_{\partial\Omega} - \int_\Omega \langle p \rangle_J \langle \nabla \cdot \mathbf{v} \rangle_J \mathrm{d}\Omega = 0, \quad \text{(S8)}$$

where $\mathrm{d}\boldsymbol{\sigma}$ is an infinitesimal oriented surface element on the boundary of the domain Ω with a direction normal to the boundary and pointing outwards. In a similar way integration by parts leads to

$$\int_\Omega \langle \mathbf{v} \rangle_J \cdot \Delta \langle \mathbf{v} \rangle_J \mathrm{d}\Omega = -\int_\Omega \left(\nabla \langle v_x \rangle_J \cdot \nabla \langle v_x \rangle_J + \nabla \langle v_y \rangle_J \cdot \nabla \langle v_y \rangle_J \right) \mathrm{d}\Omega \quad \text{(S9)}$$

and

$$\int_\Omega \langle \mathbf{v} \rangle_J \cdot \Delta^2 \langle \mathbf{v} \rangle_J \mathrm{d}\Omega = \int_\Omega \Delta \langle \mathbf{v} \rangle_J \cdot \Delta \langle \mathbf{v} \rangle_J \mathrm{d}\Omega. \quad \text{(S10)}$$

The self-adjointness of P_J allows us to drop the filter operator in the second factor in the scalar products representing the nonlinear contributions in Eq. (S7), i.e.,

$$\int_\Omega \langle \mathbf{v} \rangle_J \cdot \langle (\mathbf{v} \cdot \nabla)\mathbf{v} \rangle_J \mathrm{d}\Omega = \int_\Omega \langle \mathbf{v} \rangle_J \cdot (\mathbf{v} \cdot \nabla)\mathbf{v} \mathrm{d}\Omega, \quad \text{(S11)}$$

$$\int_\Omega \langle \mathbf{v} \rangle_J \cdot \langle |\mathbf{v}|^2 \mathbf{v} \rangle_J \mathrm{d}\Omega = \int_\Omega \langle \mathbf{v} \rangle_J \cdot (|\mathbf{v}|^2 \mathbf{v}) \mathrm{d}\Omega. \quad \text{(S12)}$$

With the aid of the decomposition of the velocity field into contributions from different spectral shells the nonlinear terms can be rewritten even further with the goal to facilitate interpretation. The Navier-Stokes nonlinearity can be represented as

$$\frac{1}{V} \int_\Omega \langle \mathbf{v} \rangle_J \cdot (\mathbf{v} \cdot \nabla)\mathbf{v} \mathrm{d}\Omega = \sum_I \frac{1}{V} \int_\Omega \langle \mathbf{v} \rangle_J \cdot (\mathbf{v} \cdot \nabla) \langle \mathbf{v} \rangle_I \mathrm{d}\Omega =: \frac{1}{\lambda_0} \sum_I T_{JI}^{\mathrm{avd}}. \quad \text{(S13)}$$

The summand in the equation above contains the contribution from two shells, S_I and S_J, and can be interpreted as the interaction between shell S_I and shell S_J. The picture of the Navier-Stokes term that arises in Fourier space is that of a three-wave coupling, i.e., a triadic interaction. The third mode/shell comes from the advective term $\mathbf{v}\cdot\nabla$. Here, we have not introduced a third index for it, i.e., we compute the interaction between the shells S_I and S_J mediated by all possible shells.
Applying the velocity decomposition on the term stemming from the cubic nonlinearity in Eq. (1) leads to

$$\frac{1}{V}\int_\Omega |\mathbf{v}|^2\langle\mathbf{v}\rangle_J\cdot\mathbf{v}\mathrm{d}\Omega = \sum_I \frac{1}{V}\int_\Omega |\mathbf{v}|^2\langle\mathbf{v}\rangle_J\cdot\langle\mathbf{v}\rangle_I\mathrm{d}\Omega =: \frac{1}{\beta}\sum_I T^{\mathrm{cub}}_{JI}, \tag{S14}$$

which, in analogy to the Navier-Stokes nonlinearity, can be interpreted as the interaction between shells S_I and S_J due to the cubic term. In this case the third 'leg' mediating the interaction is $|\mathbf{v}|^2$, i.e., the local energy density in real space. One can also look at it as two 'legs', namely one for each velocity field $\mathbf{v}$. In this case we have summed over two 'legs' in order to obtain a shell-to-shell interaction. From the summands in Eqs. (S13) and (S14) one can read off the corresponding the shell-to-shell coupling terms, namely

$$T^{\mathrm{adv}}_{IJ} = -\lambda_0\frac{1}{V}\int_\Omega \langle\mathbf{v}\rangle_J\cdot(\mathbf{v}\cdot\nabla)\langle\mathbf{v}\rangle_I\mathrm{d}\Omega \text{ and} \tag{S15a}$$

$$T^{\mathrm{cub}}_{IJ} = -\beta\frac{1}{V}\int_\Omega |\mathbf{v}|^2\langle\mathbf{v}\rangle_J\cdot\langle\mathbf{v}\rangle_I\mathrm{d}\Omega\,. \tag{S15b}$$

The equations above are equivalent to Eqs. (6a) and (6b) in the main text representing merely their real-space formulation.
Due to the symmetry of the scalar product $\langle\mathbf{v}\rangle_J\cdot\langle\mathbf{v}\rangle_I$, it is clear that T^{cub}_{IJ} is also symmetric with respect to the interchange of I and J, i.e., $T^{\mathrm{cub}}_{IJ} = T^{\mathrm{cub}}_{JI}$. On the other hand, for an incompressible velocity field and periodic boundary conditions T^{avd}_{IJ} is antisymmetric with respect to I and J. Denoting for brevity $\langle\mathbf{v}\rangle_I$ by $\mathbf{a}$, $\langle\mathbf{v}\rangle_J$ by $\mathbf{b}$ and setting $\lambda_0 = 1$, we have after integration by parts

$$\begin{aligned}
T^{\mathrm{avd}}_{IJ} &= \frac{1}{V}\int_\Omega \mathbf{a}\cdot(\mathbf{v}\cdot\nabla)\mathbf{b}\mathrm{d}\Omega = \frac{1}{V}\int_\Omega\left(a_xv_x\frac{\partial b_x}{\partial x} + a_xv_y\frac{\partial b_x}{\partial y} + a_yv_x\frac{\partial b_y}{\partial x} + a_yv_y\frac{\partial b_y}{\partial y}\right)\mathrm{d}\Omega = \\
&= \underbrace{\text{boundary terms}}_{=0} - \frac{1}{V}\int_\Omega\left(b_x\frac{\partial(a_xv_x)}{\partial x} + b_x\frac{\partial(a_xv_y)}{\partial y} + b_y\frac{\partial(a_yv_x)}{\partial x} + b_y\frac{\partial(a_yv_y)}{\partial y}\right)\mathrm{d}\Omega = \\
&= -\frac{1}{V}\int_\Omega \mathbf{b}\cdot(\mathbf{v}\cdot\nabla)\mathbf{a}\mathrm{d}\Omega - \frac{1}{V}\int_\Omega(\mathbf{a}\cdot\mathbf{b})\underbrace{(\nabla\cdot\mathbf{v})}_{=0}\mathrm{d}\Omega = -T^{\mathrm{adv}}_{JI}.
\end{aligned} \tag{S16}$$

S.3 Derivation of Eq. (7) from the Millionshchikov hypothesis

As discussed in the main text, the quasi-normal approximation rests on the Millionshchikov hypothesis [8] according to which the velocity correlations of odd order are still nonzero, but

the even-order correlations can be expressed approximately as the sum of all possible products of second-order correlations. Thus, for the fourth-order correlation in Eq. (2) we can write

$$\begin{aligned}\langle v^i_{-\mathbf{k}}(t)v^l_{\mathbf{k}-\mathbf{p}-\mathbf{q}}(t)v^l_{\mathbf{q}}(t)v^j_{\mathbf{p}}(t)\rangle = \\ = \langle v^i_{-\mathbf{k}}(t)v^l_{\mathbf{k}-\mathbf{p}-\mathbf{q}}(t)\rangle\langle v^l_{\mathbf{q}}(t)v^j_{\mathbf{p}}(t)\rangle \\ + \langle v^i_{-\mathbf{k}}(t)v^l_{\mathbf{q}}(t)\rangle\langle v^l_{\mathbf{k}-\mathbf{p}-\mathbf{q}}(t)v^j_{\mathbf{p}}(t)\rangle \\ + \langle v^i_{-\mathbf{k}}(t)v^j_{\mathbf{p}}(t)\rangle\langle v^l_{\mathbf{k}-\mathbf{p}-\mathbf{q}}(t)v^l_{\mathbf{q}}(t)\rangle. \end{aligned} \tag{S17}$$

Assuming that the system is statistically homogeneous and isotropic, the three terms on the right-hand side of the above equation can be further simplified as

$$\begin{aligned}\langle v^i_{-\mathbf{k}}(t)v^l_{\mathbf{k}-\mathbf{p}-\mathbf{q}}(t)\rangle\langle v^l_{\mathbf{q}}(t)v^j_{\mathbf{p}}(t)\rangle &= D_{il}(\mathbf{k})D_{jl}(\mathbf{p})Q_k(t)Q_p(t)\delta_{\mathbf{q},-\mathbf{p}} \\ \langle v^i_{-\mathbf{k}}(t)v^l_{\mathbf{q}}(t)\rangle\langle v^l_{\mathbf{k}-\mathbf{p}-\mathbf{q}}(t)v^j_{\mathbf{p}}(t)\rangle &= D_{il}(\mathbf{k})D_{jl}(\mathbf{p})Q_k(t)Q_p(t)\delta_{\mathbf{q},\mathbf{k}} \\ \langle v^i_{-\mathbf{k}}(t)v^j_{\mathbf{p}}(t)\rangle\langle v^l_{\mathbf{k}-\mathbf{p}-\mathbf{q}}(t)v^l_{\mathbf{q}}(t)\rangle &= D_{ij}(\mathbf{k})D_{ll}(\mathbf{q})Q_k(t)Q_q(t)\delta_{\mathbf{p},\mathbf{k}}, \end{aligned} \tag{S18}$$

where $\delta_{\mathbf{k},\mathbf{p}}$ equals one if $\mathbf{k} = \mathbf{p}$ and zero otherwise. The equal-time scalar correlation function $Q_k(t)$ is defined as $\langle v^i_{\mathbf{k}}(t)v^j_{-\mathbf{k}}(t)\rangle =: D_{ij}(\mathbf{k})Q_k(t)$ which also requires statistical isotropy. Substituting the above expressions into the term in the energy balance equation that arises from the cubic nonlinearity, we can now perform the summation over the Cartesian indices i, j and l. A preliminary computation, that proves to be useful in this regard, yields

$$\sum_j D_{jj}(\mathbf{k}) = 1, \tag{S19a}$$

$$\sum_i D_{ij}(\mathbf{k})D_{il}(\mathbf{k}) = D_{jl}(\mathbf{k}), \tag{S19b}$$

$$\sum_{i,j} D_{ij}(\mathbf{k})D_{ij}(\mathbf{k}) = 1, \tag{S19c}$$

$$\sum_{j,l} D_{jl}(\mathbf{k})D_{jl}(\mathbf{p}) = \frac{(\mathbf{k}\cdot\mathbf{p})^2}{k^2p^2} \tag{S19d}$$

for a two-dimensional setting. With the aid of the above results one can easily derive the first part of Eq. (7). For the second part of the equation, one needs to relate the scalar correlation function $Q_k(t)$ to the energy spectrum $E_{\mathbf{k}}(t)$ and perform the summation over the wave number $\mathbf{p}$. The former follows directly from the definition of the quantities and in two dimensions gives $E_{\mathbf{k}}(t) = Q_k(t)/2$. Note that, despite the vector notation of the argument, in the isotropic case $E_{\mathbf{k}}(t)$ depends only on the absolute value of the wave number. Analogously, one derives that $\sum_{\mathbf{k}} Q_k(t) = 2E_0(t)$. The contribution involving the scalar product $\mathbf{k}\cdot\mathbf{p}$ can be computed analytically in the limit of an infinitely large system, i.e., $L \to \infty$, in which the wave number becomes a continuous variable. Denoting the angle between $\mathbf{k}$ and $\mathbf{p}$ as θ, one can write

$$\begin{aligned}\sum_{\mathbf{p}} \frac{(\mathbf{k}\cdot\mathbf{p})^2}{k^2p^2}Q_p(t) = \sum_{\mathbf{p}} \cos^2(\theta)Q_p(t) \approx \int_0^{2\pi}\int_0^{\infty} \cos^2(\theta)Q_p(t)p\mathrm{d}p\mathrm{d}\theta = \\ = \frac{1}{2}2\pi\int_0^{\infty} pQ_p(t)\mathrm{d}p = \frac{1}{2}\int_0^{2\pi}\int_0^{\infty} Q_p(t)p\mathrm{d}p\mathrm{d}\phi = \frac{1}{2}\sum_{\mathbf{p}} Q_p(t) = E_0. \end{aligned} \tag{S20}$$

Taking this into account, one can easily derive the end result in Eq. (2).

In the turbulence literature one often tests how close the statistics of the velocity field is to the Gauss distribution by means of the two-point velocity increments $\delta\mathbf{v}$. The latter represent the difference in velocity at two different points separated by the vector $\mathbf{r}$. One distinguishes between longitudinal ($\parallel$) and transverse ($\perp$) velocity increments which are given by the projection of $\delta\mathbf{v}$ on the separation vector $\mathbf{r}$ and on its orthogonal complement, respectively. In mathematical terms we have that

$$\delta v_\parallel(\mathbf{x},\mathbf{r},t) = \delta\mathbf{v}\cdot\frac{\mathbf{r}}{r} = (\mathbf{v}(\mathbf{x},t)-\mathbf{v}(\mathbf{x}+\mathbf{r},t))\cdot\frac{\mathbf{r}}{r} \tag{S21}$$

$$\delta v_\perp(\mathbf{x},\mathbf{r},t) = \delta\mathbf{v}\cdot\mathbf{e}_T = (\mathbf{v}(\mathbf{x},t)-\mathbf{v}(\mathbf{x}+\mathbf{r},t))\cdot\mathbf{e}_T, \tag{S22}$$

where $\mathbf{e}_T$ is a unit vector that is perpendicular to the separation vector $\mathbf{r}$ and in terms of the unit vectors in the plane, i.e., $\mathbf{e}_1$ and $\mathbf{e}_2$, it is given by $\mathbf{e}_T = ((\mathbf{r}\cdot\mathbf{e}_2)\mathbf{e}_1 - (\mathbf{r}\cdot\mathbf{e}_1)\mathbf{e}_2)/r$. For statistically homogeneous systems the statistical properties of the velocity increments do not depend on the particular choice of the reference point $\mathbf{x}$. In addition, in the case of statistical isotropy $\delta\mathbf{v}$ will depend only on the distance r between the two points, i.e., $\delta\mathbf{v} = \delta\mathbf{v}(r,t)$. In

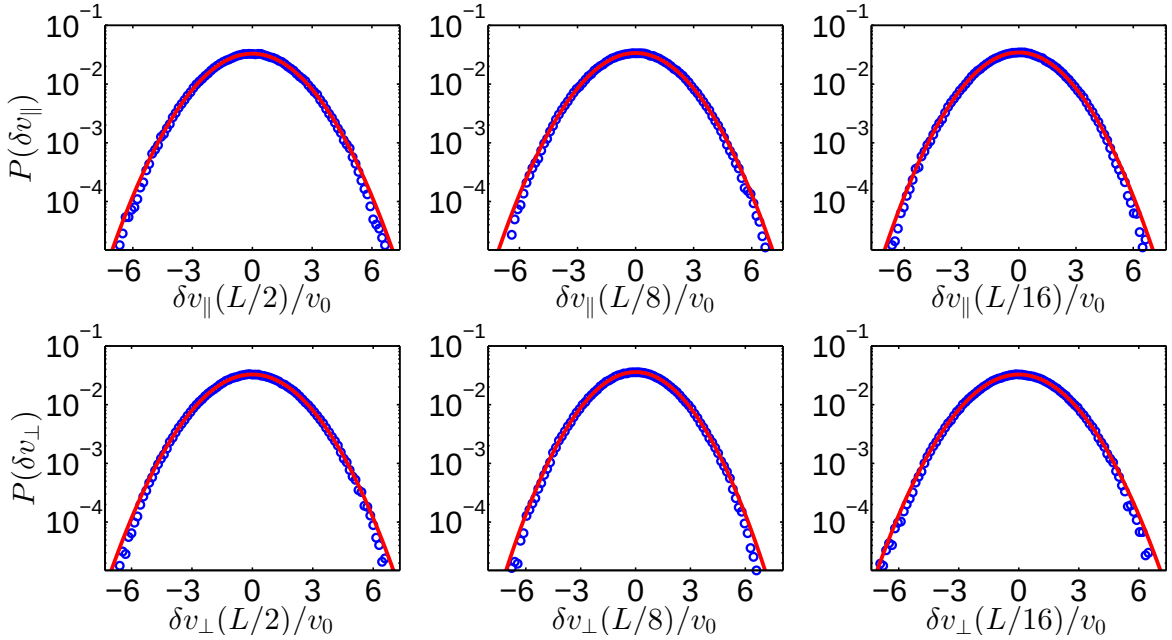

Figure 2: Numerically computed probability density function (blue circles) for the longitudinal (first row) and transverse (second row) velocity increments for three different separations: $L/2$ (first column), $L/8$ (second column) and $L/16$ (third column), where L denotes the box size of $10\pi\ell$ and the Ekman parameter is set to $\alpha\tau = -1$. The red line gives the closest fit of a Gauss distribution. Hence, the statistics of the velocity field at large scales is indeed very close to Gaussian.

the time series of $\delta v_\parallel(r,t)$ and $\delta v_\perp(r,t)$ some values will be obtained more often than others which gives us the probability distribution P of the velocity increments. (Strictly speaking, this gives us the probability density function.) A numerical computation of P (blue circles) for

the case of $\alpha\tau = -1$ is shown in Fig. 2 in a semi-logarithmic representation for three different separation vectors with the first row displaying $P(\delta v_\parallel)$ and the second one $P(\delta v_\perp)$. The red line gives the closest fit to a Gauss distribution $P(\delta v_{\parallel,\perp}) = A\exp(-\delta v^2_{\parallel,\perp}/\sigma^2)$ with A and σ being the fit parameters. As seen in the figure, the distribution of velocity increments is very close to a Gaussian at large scales which supports the use of the quasi-normal approximation. In addition, note that all the distributions in Fig. 2 have nearly the same parameters A and σ. In order to connect the results shown here to the energy spectra in wave-number space let us remark that the separations displayed in Fig. 2 correspond to $k\ell \approx 0.2$, $k\ell \approx 0.8$ and $k\ell \approx 1.6$, respectively. They all belong to the low-k range studied in this work, since, for comparison, the peak of the energy spectrum lies around $k\ell \approx 7$ for $\alpha\tau = -1$ and $k\ell \approx 15$ for $\alpha\tau = 4$. Fig. 3 displays the same probability distributions but for a different value of the constant in

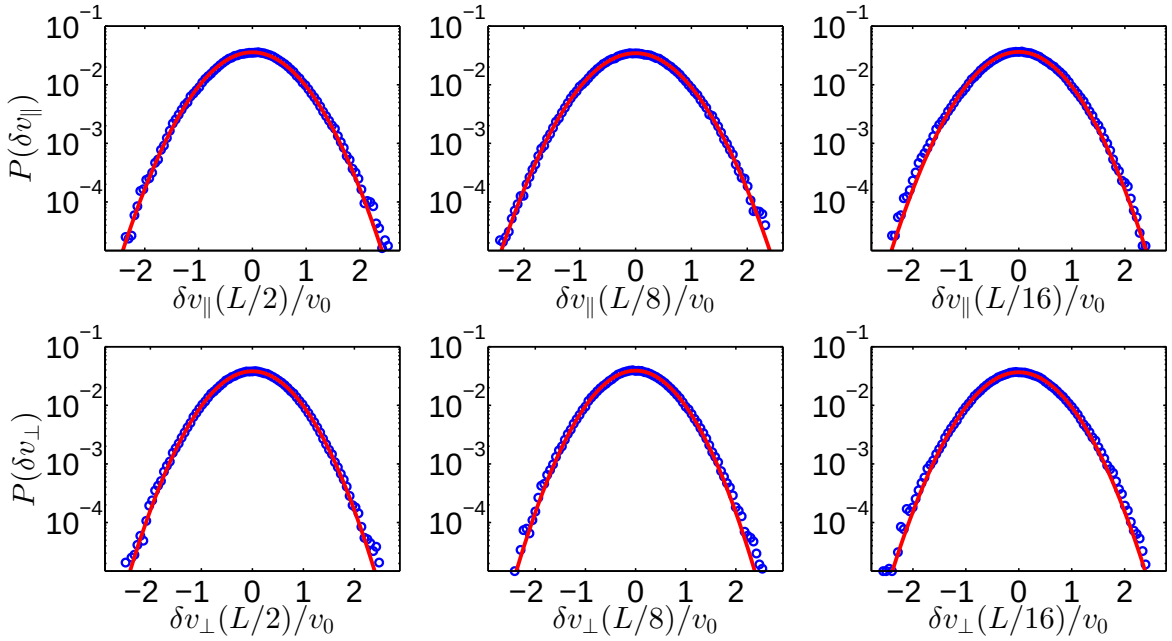

Figure 3: Numerically computed probability density function (blue circles) for the longitudinal (first row) and transverse (second row) velocity increments for three different separations: $L/2$ (first column), $L/8$ (second column) and $L/16$ (third column), where L denotes the box size of $10\pi\ell$. Here the Ekman parameter equals $\alpha\tau = 3$. The red line gives the closest fit of a Gauss distribution. The statistics of the velocity field at large scales is again very close to Gaussian.

front of the Ekman term: $\alpha\tau = 3$ which lies close to the other end of the parameter range considered here. The data leads to the same conclusion regarding the statistics of the velocity field as in the previous case for $\alpha\tau = -1$. The only difference appears to be the corresponding value of σ. Here it is considerably lower meaning that the width of the distribution is smaller. The reason for that lies in the fact that for $\alpha\tau = -1$ the Ekman term acts as an energy source while for $\alpha\tau = 3$ it dissipates energy. Thus, in the first case the total energy of the system, proportional to the integral of $|\mathbf{v}|^2$ over the whole domain, is considerably higher making larger velocity increments more probable. In conclusion, the data represented in Figs. 2 and 3 support the quasi-normal approximation we used in our analysis.

References

[1] Wensink HH *et al.* (2012) *Meso-scale turbulence in living fluids. Proc Natl Acad Sci USA* 109:14308-14313

[2] Gottlieb D, Orszag SA (1977) *Numerical analysis of spectral methods: Theory and applications.* (SIAM, Philadelphia, PA)

[3] Cooley JW, Tukey JW (1965) *An algorithm for the machine calculation of complex Fourier series. Math Comput* 19:297-301

[4] Heideman MT, Johnson DH, Burrus CS (1984) *Gauss and the history of the fast Fourier transform. IEEE ASSP Magazine* 1:14-21

[5] Cox SM, Matthews PC (2002) *Exponential time differencing for stiff systems. J Comp Phys* 176:430-455

[6] Kassam AK, Trefethen LN (2005) *Fourth-order time stepping for stiff PDES. SIAM J Sci Comput* 26:1214-1233

[7] Canuto C, Hussaini MY, Quarteroni A, Zang ThA (2011) *Spectral Methods: Fundamentals in Single Domains.* (Springer, 4th edition)

[8] Millionshchikov MD (1941) *Theory of homogeneous isotropic turbulence. Dokl Akad Nauk SSSR* 32:611-614